Fluorescence Emission of Pyrene in Surfactant Solutions

Lucas Piñeiro, Mercedes Novo, and Wajih Al-Soufi*

Department of Physical Chemistry, Faculty of Science, University of Santiago de Compostela
E-27002 Lugo (Spain), Fax: (+34) 982824001, E-mail: wajih.al-soufi@.usc.es

Abstract

The systematic description of the complex photophysical behavior of pyrene in surfactant solutions in combination with a quantitative model for the surfactant concentrations reproduces with high accuracy the steady-state and the time resolved fluorescence intensity of pyrene in surfactant solutions near the *cmc*, both in the monomer and in the excimer emission bands. We present concise model equations that can be used for the analysis of the pyrene fluorescence intensity in order to estimate fundamental parameters of the pyrene-surfactant system, such as the binding equilibrium constant K of pyrene to a given surfactant micelle, the rate constant of excimer formation in micelles, and the equilibrium constant of pyrene-surfactant quenching. The values of the binding equilibrium constant K_{TX100} = 3300 10^3 M^{-1} and K_{SDS} = 190 10^3 M^{-1} for Triton X-100 (TX100) and SDS micelles, respectively, show that the partition of pyrene between bulk water and micelles cannot be ignored, even at relatively high surfactant concentrations above the *cmc*. We apply the model to the determination of the *cmc* from the pyrene fluorescence intensity, especially from the intensity ratio at two vibronic bands in the monomer emission or from the ratio of excimer to monomer emission intensity. We relate the finite width of the transition region below and above the *cmc* with the observed changes in the pyrene fluorescence in this region.

Keywords: Surfactants · Pyrene · Critical Micelle Concentration · Fluorescence · Kinetic Description
Supporting information for this article is available on the WWW or from the author.

Contents

1 Introduction

Pyrene has been used since more than 50 years as fluorescent probe par excellence for microheterogeneous systems such as micelles [1-13], polymers [14-16], proteins [17-19], peptides [20] and biological membranes [18,21-23]. The sensitivity of the pyrene fluorescence intensity to the solvent polarity is widely used for the determination of the *cmc* of micellar systems [3,12,13,24-30]. Therefore, it is surprising that there is still no established procedure to extract a *cmc* value from pyrene fluorescence data that can be related to basic properties of the micellar system and thus be compared to results obtained from other techniques. Currently, ad hoc graphical procedures are used, such as the intersection of straight lines drawn through the experimental data at low and high surfactant concentrations or the fit of arbitrary functions that have no foundation on the well-known fluorescence properties of pyrene in micellar systems. In order to obtain a *cmc* value consistent with other techniques it is necessary to use a common definition of the *cmc* that is based on the surfactant concentration and then to deduce the response of the pyrene fluorescence to the changes in the micellar solution around the *cmc*. The difficulty to do this lies mainly in the first part, the definition of the *cmc* and the necessary model for the concentrations of monomeric and micellized surfactant around the *cmc*. Many excellent theoretical and numerical descriptions of surfactant self-aggregation [31-37] allow now to understand and to predict the properties of micellar systems, but they are still too complex to be used as models for the analysis of experimental data. As a practical solution we proposed recently a manageable model for the surfactant concentration derived from a few empirically established properties of micellar solutions around the *cmc* [38]. This model reproduces with high precision the concentrations of monomeric and micellized surfactant around the *cmc* and allows one to deduce unified descriptions for several properties that depend on these concentrations. We obtained consistent *cmc* values from different surfactant properties such as electrical conductivity, surface tension, NMR chemical shifts, absorption, and self-diffusion coefficients, and also from the fluorescence intensity and the mean translational diffusion coefficient of several fluorescent dyes in surfactant solutions [38,39]. In this contribution we combine this concentration model with the well-known photophysics of pyrene in order to obtain a manageable procedure for the analysis of the fluorescence intensity of pyrene in micellar solutions.

The photophysical behaviour of pyrene in microheterogeneous systems is complex and has been object of many detailed studies and reviews. The fluorescence spectrum of pyrene shows characteristic vibronic bands around 370 - 400 nm, whose absolute and relative intensities, width and positions depend sensitively on the polarity of the microenvironment [3,26,40-45]. The pyrene fluorescence emission can be quenched due to the diffusion controlled formation of excimers with a characteristic emission band at longer wavelengths around 500 nm [24,40,46-49]. The time dependence of the pyrene fluorescence intensity after pulsed excitation follows Stern-Volmer quenching kinetics in pure water but has a much more complex behaviour in microheterogeneous environments [26,49-53]. Although pyrene is highly hydrophobic and only sparingly soluble in pure water, it still follows a partition equilibrium between the aqueous phase and the micellar pseudophase with a partition equilibrium constant that is high but not infinite [27,39].

The ratio of the fluorescence intensities of the first and third vibronic bands of pyrene (I_I/I_{III}-ratio) increases characteristically with increasing polarity of the probe environment and defines the so called “py-scale” [42,44]. The passage of the hydrophobic pyrene from the aqueous phase to the apolar micellar pseudophase with increasing surfactant concentrations results in a sigmoidal decrease of the I_I/I_{III} -ratio around the *cmc*. Although visually very suggestive, there is not one special point of the sigmoid which can be directly assigned to the *cmc* of the solution, especially not the centre of the sigmoid. Zana et al. [27] gave a special solution for the limiting case of zero *cmc* taking into account the partition equilibrium of pyrene between aqueous and micellar phase. Aguiar et al. proposed to use the relative width of the sigmoidal as a criterion for the selection of one of two possible *cmc* values: the centre of the sigmoid in the case of nonionic surfactants and the intersection of two straight lines drawn through the rapidly changing part and the horizontal part at high concentrations for ionic surfactants with higher *cmc* values [30]. This leads to *cmc* values that are in agreement with those obtained with other techniques. However, this phenomenological approach does not take into account the partition equilibrium of pyrene and does not relate the sigmoidal model and its parameters with more fundamental physical properties of the system under study. It is not clear why any of the two selected concentrations should represent the same *cmc* as determined with other techniques.

Pyrene excimer formation is another property that is highly sensitive to the formation of the first micelles around the *cmc* [8,52,54,55]. Due to the low solubility of pyrene in pure water, the efficiency of excimer formation is low at surfactant concentrations below the *cmc*. The same is true at high surfactant concentrations where there is a very low probability to find more than one pyrene molecule in a micelle. However, at the *cmc* the pyrene molecules are crowded into the first few micelles so that excimer formation is favoured and leads to a relatively strong peak in the excimer fluorescence intensity. Again, this peak does not coincide with the *cmc* itself and the quantitative analysis of the excimer fluorescence for the determination of the *cmc* has not been fully achieved yet.

Misra et al. interpret the fact that the excimer peak appears at concentrations below the *cmc* as evidence for the formation of pre-micellar aggregates and the gradual decrease of the I_1/I_3-ratio as a progressive increase of the micellar size [56]. As we will show here, both observations can be readily explained taking into account the partition equilibrium of pyrene and the finite size of the transition

region around the *cmc* without the need for pre-micelles or a step-wise growth of micellar size.

A full description of the dependence of the pyrene fluorescence intensity and decay on the surfactant concentration near the *cmc* has to take into account several processes (Scheme 1): (1) the concentration of monomeric surfactant and micelles for a given total surfactant concentration (the surfactant-concentration model), (2) the partition equilibrium of pyrene between bulk water and micelles, (3) the distribution of bound pyrene among the micelles, (4) the quenching of pyrene due to excimer formation and (5) the interaction of pyrene with monomeric surfactant. We will combine these processes step by step and then apply the resulting equations to experimental data.

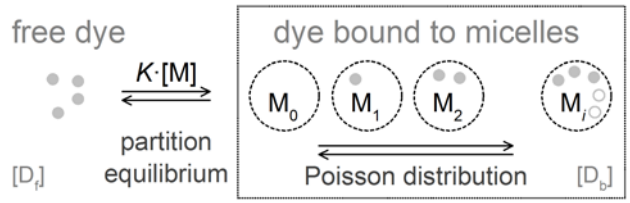

Scheme 1: Processes controlling the dependence of the pyrene fluorescence intensity and decay on the surfactant concentration near the *cmc*. Free dye (D_f) partitions between bulk water and micelles with binding equilibrium constant *K*. The distribution of the bound dye (D_b) among the micelles leads to different local dye concentrations in micelles M_i with occupancy *i*. Not shown here is the quenching of free dye by surfactant molecules and the formation of dye excimers in the micelles.

2 Theory

We distinguish three dominant fluorescent pyrene species in a micellar solution: free pyrene in the aqueous phase emitting as monomer (D_f), and pyrene bound to micelles emitting as monomer (D_{bm}) or emitting as excimer (D_{be}) (see Fig. SI2 in the SI). We ignore the very weak contribution of the excimer formed by free pyrene in water.

At a given emission wavelength λ the total observed fluorescence intensity $I^{(\lambda)}$ is the sum of the contributions of each of the species:

$$I^{(\lambda)} = F_f^{(\lambda)}[\mathrm{D_f}] + F_{bm}^{(\lambda)}[\mathrm{D_{bm}}] + F_{be}^{(\lambda)}[\mathrm{D_{be}}] \qquad (1)$$

This expression for the fluorescence intensity applies both in the so called "monomer" and in the "excimer" bands of the pyrene emission spectrum, with varying contributions of the species depending on the wavelength. In the "monomer" band the emission is dominated by free and bound monomeric (F_f, F_{bm}) pyrene with a residual emission of the pyrene excimer. In the "excimer" band the situation is just reversed, with a strong contribution of the excimer (F_{be}).

The task is now to obtain reasonable model equations for the concentrations of the species (D_f, D_{bm}, and D_{be}) as a function of the total surfactant concentration $[S]_0$. A rigorous kinetic description of the pyrene fluorescence in detergent micelles was given by Infelta and Grätzel [5]. We combine their results with our surfactant concentration model, introduce the interaction between pyrene and surfactant monomers observed at low surfactant concentrations and derive and discuss expressions for cases relevant for the determination of the *cmc*. We also derive equations for the time dependency of pyrene fluorescence. In the following we present the steps in a systematic way.

2.1 Surfactant Concentration Model

The established model to calculate the concentration of micelles in solution $[M] = ([S]_0 - cmc)/n$ from the total surfactant $[S]_0$, the *cmc*, and the aggregation number *n*, works well above the *cmc* region, but is not defined in the important region below and near the *cmc*. Recently we introduced an improved surfactant-concentration model that has proven to provide an excellent basis for a variety of derived direct properties of a surfactant solution around the *cmc* and also for the fluorescence intensity and mean translational diffusion of fluorescent probes in micellar solutions [38,39]. The model is still compact enough to be easily implemented in standard fitting software for routine data analysis.

At low $[S]_0$ monomeric surfactants dominate whereas at high $[S]_0$ micelles determine the properties of the solution. The transition between these regions around the *cmc* is not abrupt but gradual within a transition concentration interval with width σ, given by the width of a Gauss function that describes the second derivative (curvature) of $[S_1]$ with respect to $[S]_0$ (see SI). The smaller σ is the sharper is the transition between the two linear regions below and above the *cmc*. In order to facilitate the comparison of widths σ between surfactants with different *cmc* values, we define the relative transition width *r* as:

$$r = \sigma / cmc \qquad (2)$$

Our model (eq. (3)) for the concentration of surfactant monomers $[S_1]$ in a solution with total surfactant concentration $[S]_0$ is based on the "Phillips-condition" [57] and has the form of adequately normalized sigmoidal function centred around the *cmc* and with relative transition width *r* and the relative concentration $s_0 = [S]_0/cmc$ [38,39]:

$$[S_1] = cmc\left[1 - \frac{A}{2}\left(\sqrt{\frac{2}{\pi}}\, r \exp\left(-\frac{(s_0-1)^2}{2r^2}\right) + (s_0-1)\left(\mathrm{erf}\left(\frac{s_0-1}{\sqrt{2}r}\right) - 1\right)\right)\right] \qquad (3)$$

where *A* is the normalization constant (for small *r* <0.5: A≈1):

$$A = \frac{2}{1 + \sqrt{\frac{2}{\pi}}\, r \exp\left(-\frac{1}{2r^2}\right) + \mathrm{erf}\left(\frac{1}{\sqrt{2}\, r}\right)} \approx 1 \qquad (r < 0.5) \qquad (4)$$

The concentration of aggregated (micellized) surfactants, $[S_m]$, is the difference between the total concentration and that of monomeric surfactants:

$$[S_m] = [S]_0 - [S_1] \qquad (5)$$

The concentration of micelles, [M], depends on the mean aggregation number *n*, which is taken to be constant around the *cmc*:

$$[\mathrm{M}] = [\mathrm{S_m}] / n \qquad (6)$$

Fig. 1-a shows simulated data of $[S_1]$ and $[S_m]$ and the Gaussian function with width *r* calculated with the concentration model (eqs. (3) to (5)) for three typical values of the relative transition width *r*. Details of the surfactant concentration model (eqs. (3) to (6)) have been discussed before and are given in the SI [38].

The concentration of micelles formed already below the *cmc* increases with the relative transition width *r* (see Fig. 1-a). For typical small values of *r* ($r<0.5$) the fraction of micellized surfactants $[S_m]/[S]_0$ at the *cmc* is $[S_m](cmc)/cmc \approx r/\sqrt{2\pi} \approx 0.4r$ and thus the micelle concentration at the *cmc* is given by:

$$[\mathrm{M}](cmc) \approx \frac{cmc}{n}\frac{r}{\sqrt{2\pi}} = \frac{1}{n}\frac{\sigma}{\sqrt{2\pi}} \approx 0.4\frac{\sigma}{n} \qquad (7)$$

The polydispersity of real surfactant samples is not explicitly taken into account but is captured by the relative transition width r. For example, the conductivity of the polydisperse surfactant mixture LAS is well described by the model with an atypically high value of *r* of 0.48 [38].

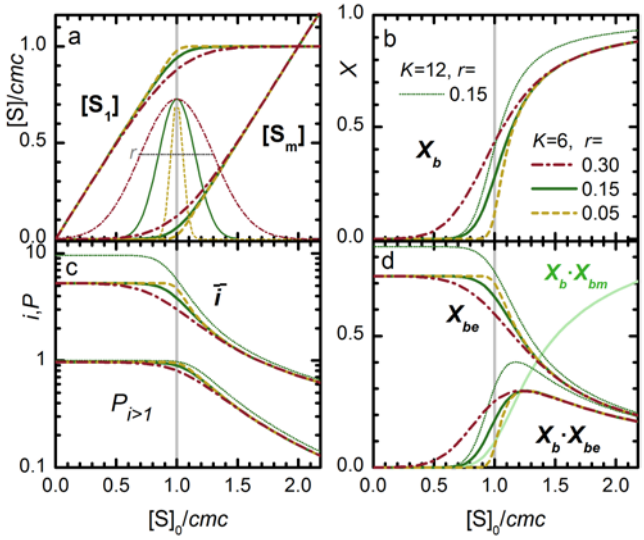

Fig.1: Relative concentrations $[S_1]/cmc$, $[S_m]/cmc$, molar fractions X_b, X_{be}, $X_b \cdot X_{be}$, mean occupancy $\bar{i}$ and occupancy probability $P(i>1)$ versus relative surfactant concentration $s_0 = [S_0]/cmc$ for different values of *r* and *K* as indicated. The thin lines in panel a are Gaussians with width *r* and arbitrarily normalized amplitude. (Values used for the simulations: $cmc=0.275$, $n=143$, $K=3300$ and 6000, $[D]_0 = 1.6\ 10^{-3}$, $K_q=2.2$, $K'_{be}=0.6$). The value of *K* is normalized to $K \cdot cmc/n$.

2.2 Binding Equilibrium

Near the *cmc* pyrene coexist in the aqueous phase and in the micellar pseudophase with concentrations of free and bound pyrene given by a 1:1 binding equilibrium as shown in eq.(8), with an apparent (macroscopic) binding equilibrium constant *K* [4,27,39,58-60]. Some authors prefer the term "partition equilibrium". However, the binding equilibrium constant *K* should not be confounded with a partition constant of a phase equilibrium [61].

$$\mathrm{D_f} + \mathrm{M} \overset{K}{\rightleftharpoons} \mathrm{D}_b \qquad K = \frac{[\mathrm{D_b}]}{[\mathrm{D_f}][\mathrm{M}]} \qquad (8)$$

The molar fractions of free (X_f) and bound dye (X_b) with respect to the total dye concentration $[D]_0 = [D_f] + [D_b]$ are given by eq. (9). The fraction of bound dye X_b near the *cmc* is shown in Fig. 1-b for different values of *r* and *K*. Both *K* and *r* determine X_b. For a given value of $K=6$ (thick lines) an increasing transition width *r* moves the onset of the transition region towards lower concentrations (to about $cmc-2\sigma$ or $1-2r$ in this scale) and thus also, the onset of the increase in X_b. With increasing *r* the concentration of dye bound to micelles already below the *cmc* increases. Comparing two values of *K* ($K=6$ and $K=12$) at the same $r=0.15$, the onset of the change in X_b coincides, but the change is faster for the higher *K*. In any case, both parameters affect X_b in a rather similar way and are therefore correlated in nonlinear fits.

$$X_f = \frac{[\mathrm{D_f}]}{[\mathrm{D}]_0} = \frac{1}{1+K\cdot[\mathrm{M}]}, \quad X_b = \frac{[\mathrm{D_b}]}{[\mathrm{D}]_0} = \frac{K\cdot[\mathrm{M}]}{1+K\cdot[\mathrm{M}]} \qquad (9)$$

2.3 Dye Distribution

The mean number of pyrene molecules per micelle (mean occupancy $\bar{i}$) is given by the ratio of the concentrations of bound pyrene and micelles:

$$\bar{i} = \frac{[\mathrm{D_b}]}{[\mathrm{M}]} = \frac{\sum_{i=0}^{\infty} i\cdot[\mathrm{M_i}]}{\sum_{i=0}^{\infty}[\mathrm{M_i}]} = K[\mathrm{D_f}] = [\mathrm{D}]_0 \cdot K \cdot X_f \qquad (10)$$

At very low surfactant concentration (and consequently low [M] and $[D_b]$) the mean occupancy $\bar{i}$ starts at a limiting value of $\bar{i} \le K\cdot[\mathrm{D}]_0$, and then decreases proportionally to the fraction of free dye X_f as the micelle concentration increases (see Fig. 1-c). Again *K* and *r* have subtly different influence on the mean occupancy $\bar{i}$. With a broader transition width *r* the mean occupancy $\bar{i}$ decreases already at lower surfactant concentrations [S]. Higher values of *K* move the whole curve up to higher values of $\bar{i}$.

The distribution of bound pyrene among the micelles is sufficiently well described by a Poisson distribution [5,26,62-65]. The probability P_i that a micelle is occupied by *i* pyrene molecules (in a micelle M_i) depends on the mean occupancy of the micelles $\bar{i}$ as in eq. (11).

$$P_i = \frac{[\mathrm{M_i}]}{[\mathrm{M}]} = \frac{\bar{i}^{\,i} e^{-\bar{i}}}{i!} \qquad (11)$$

Fig. 1-c shows the probability $P_{i>1}$ that micelles are occupied by two or more dye molecules.

2.4 Excimer Formation

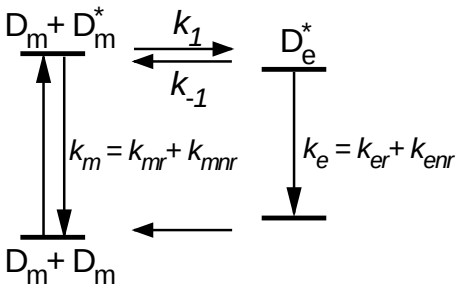

Scheme 2: Mechanism of the formation of excimer D_e^* with rate constants k_1 and k_{-1} after excitation of the monomeric dye D_m. The deactivation rate constants of monomeric dye (k_m) and excimer (k_e) are sums of radiative (k_{mr}, k_{er}) and non-radiative rate constants (k_{mnr}, k_{enr}).

The differential equations describing the dynamics of the excimer formation of pyrene in micelles have been presented by Infelta et al. and other authors [5,47,52]. The equations for the case of a homogeneous pyrene solution without surfactants is presented in the SI. Here we show briefly the results in a micellar solution with bound pyrene. The detailed derivation is given in the SI.

An excited monomeric dye D_m^* can either deactivate directly to the ground state or it can form the excimer D_e^* interacting with an unexcited monomeric dye D_m, as shown in Scheme 2. The lifetimes of the excited monomer is $\tau_m = (k_m + k_1[D_m])^{-1}$ and that of the excimer $\tau_e = (k_e)^{-1}$.

In a micellar solution both free and bound pyrene contribute to the observed fluorescence intensity (eq. (1)). Free pyrene in water forms only a very small fraction of excimer D_{fe}, which we neglect in our model ($[D_{fe}] \approx 0$, $[D_{fm}] \approx [D_f]$). This free excimer D_{fe} could, however, be easily included in the model. On the contrary, the contribution of the excimer emission from pyrene bound to micelles is important and has to be modelled carefully taking into account the local pyrene concentration given by the occupancy i of the micelles.

Without back reaction in the excited state ($k_e \gg k_{-1}$), the fraction of bound excited dye in micelles M_i that decays as monomers ($X_{bm}^{(i)}$) or excimers ($X_{be}^{(i)}$) is given by:

$$X_{bm}^{(i)} = \frac{1}{1 + K'_{be}(i-1)} \qquad X_{be}^{(i)} = 1 - X_{bm}^{(i)} \tag{12}$$

The fraction of bound excimer $X_{be}^{(1)}$ is zero for a micelle M_1 occupied by only one dye molecule and increases with higher occupation numbers. The constant K_{be} of the formation of excimer in micelles is given by the rate constants of excimer formation k_1 and of the monomer deactivation k_m and is taken to be independent of the occupancy of the micelle:

$$K_{be} = \frac{k_1}{k_m} \qquad K'_{be} = \frac{K_{be}}{V_m} \tag{13}$$

The volume V_m contains the dye bound to a micelle and defines the local concentration of not excited dye in a micelle M_i: $[D_{bm}]^{(i)} = (i-1)/V_m$. This volume is included in the constants $K'_{be} = K_{be}/V_m$ and $k'_1 = k_1/V_m$. Neither the constant K_{be} nor the volume V_m depend on $[S]_0$ as long as the structure and the size of the micelles do not change significantly.

The total steady state fluorescence intensities I_{bm} and I_{be} of bound monomer and excimer are then given by the sum of the intensities from micelles with different occupation numbers (see SI):

$$I_{bm} = F_{bm} X_{bm} X_b [D]_0, I_{be} = F_{be} X_{be} X_b [D]_0 \tag{14}$$

with the fraction X_b of bound dye (eq. (9)), and the monomer and excimer fractions of bound dye X_{bm} and X_{be}:

$$X_{bm} = e^{-\bar{i}} \sum_{i=0}^{\infty} \frac{1}{1 + iK'_{be}} \frac{\bar{i}^i}{i!}, X_{be} = 1 - X_{bm} \tag{15}$$

As can be seen in Fig. 1-d the excimer fraction of bound dye X_{be} decreases with increasing surfactant concentration following the decreasing mean occupation number. However, more relevant, the overall fraction of bound dye emitting as excimer $X_b X_{be}$ shows a sharp maximum near the cmc. This excimer fraction increases at the beginning of the transition region as the first bound dye appears (increasing X_b, high $\bar{i}$), passes through a maximum near the *cmc* and then decays as $\bar{i}$ gets smaller. The peak in $X_b X_{be}$ results from the competition of two effects. On the one hand, the fraction of bound dye X_b increases as the first micelles appear; on the other hand, the probability that this bound dye emits as excimer (X_{be}) decreases with the surfactant concentration since it is distributed among more micelles with decreasing occupancy $\bar{i}$. The form of $X_b X_{be}$ curve and the position of its maximum depend sensitively and in a complex manner on both on r and K.

It is worth noting, that the peak in this curve does not simply results "from the passage of $\bar{i}$ through a maximum after which all the pyrene in the system is solubilized in micelles", as previously reported [66]. The occupancy $\bar{i}$ has no maximum and, more important, the fraction of bound (solubilized) pyrene X_b is still far from reaching saturation (X_b =1) at the maximum of the $X_b X_{be}$ curve (see Fig. 1-d). Full solubilisation of pyrene is only reached asymptotically at high surfactant concentrations that depend, of course, on the value of K (see also Figs. 3, 5, 6)

2.5 Pyrene-Surfactant Quenching

The emission of dyes may be quenched by surfactant molecules and their counterions [60]. Pyrene is a neutral probe and does not show the complex behaviour observed for charged dyes and ionic surfactants, as for example for the cationic dye Rhodamine 123 [60]. In this section we describe the observed decrease of the pyrene fluorescence below the *cmc* as a static and/or dynamic quenching process. We discuss the quenching process in section 3.3

on the basis of steady-state and time-resolved fluorescence data.

The contribution to the fluorescence intensity $I_f^{(\lambda)}$ of the unquenched free dye can be expressed by the fraction of *not quenched* dye X_{nq} and the total concentration of free monomeric dye $[\mathrm{D_f}] = X_f [\mathrm{D}]_0$:

$$I_f^{(\lambda)} = F_f^{(\lambda)} X_{nq} X_f [\mathrm{D}]_0 \tag{16}$$

If both static and dynamic quenching occur the fraction $X_{nq} = \left(\left(1+K_{qs}[\mathrm{S_1}]\right)\left(1+K_{qd}[\mathrm{S_1}]\right)\right)^{-1}$ is second order in $[\mathrm{S_1}]$ with the quenching constants K_{qs} and K_{qd} of static and dynamic quenching, respectively.

In the case that one of the two quenching processes dominates a first order fraction with quenching constant K_q is sufficient:

$$X_{nq} = \left(1+K_q[\mathrm{S_1}]\right)^{-1} \tag{17}$$

The nature of the dominant quenching process has to be determined from additional information such as time-resolved fluorescence data.

Above the transition region the fraction becomes constant $X_{nq} = (1+K_q \cdot cmc)^{-1}$.

The same quenching formalism applies to the pyrene species bound to micelles, $\mathrm{D_{bm}}$ and $\mathrm{D_{be}}$. However, the quenching of these species depends on the *local* concentration of surfactant and on the microviscosity within the micelles. The size and structure of micelles do not significantly change within the concentration range studied here, and, therefore, within a micelle, both the quenching constant K_q and the local surfactant concentration $[\mathrm{S_m}]_{local} \approx n/V_m$ should be independent from the total surfactant concentration. Then, the fraction of quenched bound dye is constant and can be included in the constants F_{bm} and F_{be}.

2.6 Steady-State Fluorescence Intensity

Finally we can express the overall observed fluorescence intensity $I^{(\lambda)}([\mathrm{S}]_0)$ as a function of the total surfactant concentration substituting in eq. (1) the individual contributions deduced above:

$$I^{(\lambda)} = I_{f,nq}^{(\lambda)} + I_{bm}^{(\lambda)} + I_{be}^{(\lambda)} = F_f^{(\lambda)}[\mathrm{D}]_0 \left(X_f X_{nq} + q_{bm,f}^{(\lambda)} X_b X_{bm} + q_{be,f}^{(\lambda)} X_b X_{be} \right) \tag{18}$$

Here we define brightness ratios q of the fluorescence intensities of bound monomer and excimer with respect to free dye at a given wavelength λ (see Fig.2-a):

$$q_{bm,f}^{(\lambda)} = \frac{F_{bm}^{(\lambda)}}{F_f^{(\lambda)}},\ q_{be,f}^{(\lambda)} = \frac{F_{be}^{(\lambda)}}{F_f^{(\lambda)}} \tag{19}$$

Together with the concentration model of eqs (3)-(6) eq. (18) describes the fluorescence intensity of pyrene in micellar solutions as a function of total surfactant concentration with model parameters *cmc*, *r*, *n*, *K*, $F_f^{(\lambda)}$, $q_{bm,f}^{(\lambda)}$, $q_{be,f}^{(\lambda)}$, K_q, K'_{be}, and $[\mathrm{D}]_0$. The total dye concentration $[\mathrm{D}]_0$ and the aggregation number *n* are usually known. The fluorescence intensity of free dye in pure water $F_f^{(\lambda)}[\mathrm{D}]_0 = I^{(\lambda)}([\mathrm{S}]_0 = 0) \equiv I_f^{(\lambda)}$, and the ratio $q_{bm,f}^{(\lambda)}$ can be determined from the intensities at zero and at high micelle concentrations, respectively. The other parameters (*cmc*, *r*, *K*, K_q, K'_{be}, *and* $q_{be,f}^{(\lambda)}$) have to be determined by nonlinear fit.

Traditionally not the absolute intensity of the pyrene emission is analysed but the *spectral ratio SR* at two wavelengths, λ_1 and λ_2, for example the monomer/monomer (I_I/I_{III}) ratio ("py-scale" [42,44]) or excimer/monomer ratios. We distinguish here between the "spectral ratio" $SR^{(2,1)} = I^{(2)}/I^{(1)}$ of the fluorescence intensities at two wavelengths of the same species and the "brightness ratio" q of the intensities of two different species (eg. free and bound) at the same wavelength.

With eq. (18) we obtain for the spectral ratio at λ_1 and λ_2:

$$SR^{(2,1)} = \frac{I^{(2)}}{I^{(1)}} = \frac{F_f^{(2)} X_f X_{nq} + F_{bm}^{(2)} X_b X_{bm} + F_{be}^{(2)} X_b X_{be}}{F_f^{(1)} X_f X_{nq} + F_{bm}^{(1)} X_b X_{bm} + F_{be}^{(1)} X_b X_{be}} \tag{20}$$

Neglecting the residual excimer emission in the monomer band and vice versa, we get the following two expressions for the spectral monomer-monomer and excimer-monomer ratios (see SI):

$$SR_m^{(2,1)} = \frac{I^{(2)}}{I^{(1)}} \approx \frac{SR_f^{(2,1)} X_f X_{nq} + SR_{bm}^{(2,1)} q_{bm,f}^{(1)} X_b X_{bm}}{X_f X_{nq} + q_{bm,f}^{(1)} X_b X_{bm}}$$

$$SR_e^{(e,m)} = \frac{I^{(e)}}{I^{(m)}} \approx \frac{SR_f^{(e,m)} X_f X_{nq} + SR_{bm}^{(e,m)} q_{bm,f}^{(m)} X_b X_{bm} + q_{be,f}^{(e,m)} X_b X_{be}}{X_f X_{nq} + q_{bm,f}^{(m)} X_b X_{bm}} \tag{21}$$

The limiting values of the monomer-monomer ratio $SR_m^{(1,2)}$ are the spectral ratios of free pyrene, $SR_f^{(2,1)}$ at $[\mathrm{S}]_0 = 0$, and of bound monomeric pyrene, $SR_{bm}^{(2,1)}$ at $[\mathrm{S}]_0 \gg cmc$ (see Fig.2):

$$SR_f^{(2,1)} = \frac{F_f^{(2)}}{F_f^{(1)}} \qquad SR_{bm}^{(2,1)} = \frac{F_{bm}^{(2)}}{F_{bm}^{(1)}}$$

$$SR_f^{(e,m)} = \frac{F_f^{(e)}}{F_f^{(m)}} \qquad SR_{bm}^{(e,m)} = \frac{F_{bm}^{(e)}}{F_{bm}^{(m)}} \tag{22}$$

$$q_{be,f}^{(e,m)} = \frac{F_{be}^{(e)}}{F_f^{(m)}}$$

At very low pyrene concentrations the excimer formation can be neglected in eq. (21) ($X_{bm} \approx 1$, $X_{be} \approx 0$). Below the transition region $SR_m^{(2,1)} \approx SR_f^{(2,1)}$, independently of the quenching fraction X_{nq}. Above the transition region X_{nq} is constant. With the constant $c = q_{bm,f}^{(1)} K (1+K_q \cdot cmc)$ and not too high values of *r* we get a further simplified equation for $SR_m^{(2,1)}$ (see SI):

$$SR_m^{(2,1)} \approx \frac{SR_f^{(2,1)} X_{nq} + SR_{bm}^{(2,1)} q_{bm,f}^{(1)} K[\mathrm{M}]}{X_{nq} + q_{bm,f}^{(1)} K[\mathrm{M}]} \approx \frac{SR_f^{(2,1)} + SR_{bm}^{(2,1)} c[\mathrm{M}]}{1 + c[\mathrm{M}]} \tag{23}$$

Around the *cmc* both the absolute intensities $I^{(\lambda)}$ and the spectral ratios $SR_m^{(2,1)} = I^{(2)}/I^{(1)}$ and $SR_e^{(e,m)} = I^{(e)}/I^{(m)}$ depend sensitively on the interplay between the binding equilibrium constant K and the occupancy i (see Fig.2-b and c). The intensities and the spectral ratios follow the fractions X_f, $X_b \cdot X_{bm}$, *and* $X_b \cdot X_{be}$ discussed above (Fig. 1). Note that the curves of the intensities and those of the spectral ratios are significantly different, with different positions of the inflection points of the monomer curves and of the peaks of the excimer signals. The *cmc* does not correspond to any of these special points, but its relative position depends again on the values of K and r. It is also important to note, that neither of these curves has the exact form of a sigmoidal Boltzmann function.

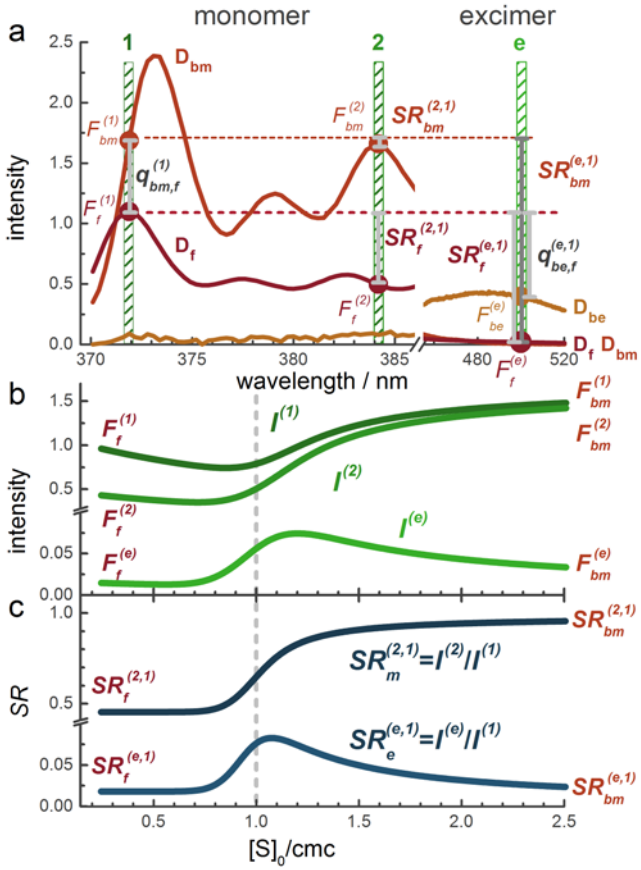

Fig.2: a) Detail of the pyrene spectrum with the spectral parameters used in the text. b) Simulated fluorescence intensity $I^{(\lambda)}([\mathrm{S}]_0)$ of eq. (18) at three wavelengths 372 nm (1), 384 nm (2), and 500 nm (e) as indicated in a). c) simulated spectral ratios $SR_f^{(2,1)}$ and $SR_{bm}^{(2,1)}$ of eq. (21) at the three wavelength 1,2, and e as indicated in a).

2.7 Time-Resolved Fluorescence Intensity

The time dependence of the pyrene fluorescence had been derived by Tachiya, by Selinger and Watkins, and by Infelta et al. [5,47,50,52,67]. We summarize the main results in our nomenclature and combine them with our surfactant concentration model. The detailed derivation can again be found in the SI.

The observed time dependent fluorescence intensity is the sum of the contributions $(i_{bm}^{(i)}(t),\ i_{be}^{(i)}(t))$ from micelles $\mathrm{M_i}$ with different occupation numbers i:

$$I_{bm}(t) = \sum_{i=1}^{\infty} i_{bm}^{(i)}(t) = F_{bm}[\mathrm{D}]_b\, \mathrm{e}^{-\bar{i}} \sum_{i=0}^{\infty} \frac{\bar{i}^i}{i!} \exp\left(-\left(k_m(1+K'_{be}\, i)t\right)\right)$$
$$I_{be}(t) = \sum_{i=1}^{\infty} i_{be}^{(i)}(t) = F_{be}[\mathrm{D}]_b\, \mathrm{e}^{-\bar{i}} \sum_{i=0}^{\infty} \frac{\bar{i}^i}{i!} \frac{K'_{be}\, i}{1 + K'_{be}\, i - k_e/k_m} \left(\exp(-k_e\, t) - \exp\left(-\left(k_m(1+K'_{be}\, i)t\right)\right)\right) \tag{24}$$

The fluorescence intensity in the monomer band $I_{bm}(t)$ can be solved analytically ($K'_{be} = K_{be}/V_m$, $k'_1 = k_1/V_m$):

$$I_{bm}(t) = F_{bm}[\mathrm{D_b}] \exp\left(\bar{i}\left(\exp\left(-K'_{be} k_m\, t\right) - 1\right) - k_m\, t\right) = F_{bm}[\mathrm{D_b}] \exp\left(\bar{i}\left(\exp\left(-k'_1\, t\right) - 1\right) - k_m\, t\right) \tag{25}$$

The analytical expression for the excimer intensity $I_{be}(t)$ is less useful for numerical applications (see SI). In fitting functions it is more reliable to calculate the sums in eq.(24) up to some reasonable occupation number i.

Note that $I_{bm}(t)$ is not monoexponentially with a lifetime $\tau_m = (k_m + k_1[\mathrm{D}_m])^{-1}$ as one would expect in a homogeneous solution. The excimer formation with $k_1[\mathrm{D}_{bm}^{(i)}]$ depends on the local dye concentration $[\mathrm{D}_{bm}^{(i)}]$, which varies according to the distribution of the dye among in the micelles. In each micelle $\mathrm{M_i}$ the excited dye decays with a different lifetime $\tau_{bm}^{(i)} = (k_m + k_1[\mathrm{D}_{bm}^{(i)}])^{-1}$. In higher occupied micelles the monomer emission is rapidly quenched due to the effective excimer formation leading to fast decays. At t=0 the decay starts with a rate constant $k_m + k_1(\bar{i}/V) = k_m(1 + K'_{be}\bar{i})$. At longer times $(K'_{be} k_m t \gg 1)$ finally only the emission from micelles $\mathrm{M_1}$ with a single excited dye is observed that decays monoexponentially with $\tau_{bm}^{(1)} = (k_m)^{-1}$. The time dependence in eq. (25) can be easily confounded with a double exponential decay with $\tau_{bm}^{(1)} = (k_m)^{-1}$ and a short lifetime, which has no explanation in a homogeneous system (see Fig. SI1 in SI).

The monomer decay $I_{bm}(t)$ in eq. (25) is furthermore strongly dependent on the micellar concentration. First, trivially, because the concentration of bound dye $[\mathrm{D_b}]$ depends on [M] (eq. (9)). Second, and more important, because the mean occupancy $\bar{i}$ in the exponent of $I_{bm}(t)$ varies with both $[\mathrm{D_b}]$ and [M] (eq.(10)). At high micellar concentrations $([\mathrm{S}]_0 \gg cmc)$ the mean occupancy tends to zero $(\bar{i} = [D_b]/[M] \to 0)$ and $I_{bm}(t)$ decays monoexponentially with k_m. At very low micellar concentrations the mean occupancy is limited by $\bar{i} \le [\mathrm{D}]_0 \cdot K$ (eq. (10)), although the amplitude of the decay vanishes. The expression of eq. (25) can be used directly as fitting function for $I_{bm}(t)$.

The excimer fluorescence intensity $I_{be}(t)$ is zero at time zero, $I_{be}(t=0) = 0$ and increases with a complex time dependent rise time given by that of the monomer decay as discussed before. At long times the decay is

monoexponential with k_e. However, at intermediate times the intensity curve follows a more complex function than the difference between excimer and monomer decays.

So finally the time resolved fluorescence emission $I(t)$ is given by the sum of the contributions of free dye (τ_f), bound monomer $I_{bm}(t)$ (eq. (25)), and bound excimer $I_{be}(t)$ (eq.(24)). Additionally a small contribution of surfactant fluorescence (for example in TX100) and/ro fluorescent impurities with typically short lifetime (τ_s) is added. The amplitudes A_x contain all constant pre-exponential factors.

$$I(t) = A_s\, e^{-t/\tau_s} + A_f\, e^{-t/\tau_f} + A_{bm} I_{bm}(t) + A_{be} I_{be}(t) \qquad (26)$$

3 Results and Discussion

3.1 Steady-State Fluorescence Intensity

Fig.3 shows spectra and profiles of the fluorescence intensity for pyrene in aqueous solutions of increasing concentrations of TX100. The spectrum of pyrene at the lowest TX100 concentration (black curve in panel A, [TX100] = 0.03mM) presents the known vibronic structure in the monomer band between 370 and 450 nm and no measurable excimer emission above 480 nm. At TX100 concentrations up to about 0.2 mM the fluorescence intensity decreases without significant change in the shape of the spectra. Above 0.2 mM a red-shift of the monomer band of nearly 2 nm and a strong increase of its intensity is observed. Around 0.3 mM a small and broad excimer emission appears with a maximum at 500 nm. The dependence of the fluorescence intensity in the first (I_I at 372 nm) and in the third vibronic band (I_{III} at 384 nm) and in the excimer band (I_e at 500 nm) on [TX100] is shown in panel B of Fig. 3. Below the *cmc* the fluorescence intensity in the monomer band (I_I and I_{III}) decreases and reaches a minimum around 0.22 mM. Near the *cmc* this intensity increases strongly until it reaches about twice the initial value at concentrations above 1 mM.

In the excimer band (I_e) the fluorescence emission is nearly zero below the *cmc*. Around the cmc the excimer intensity increases sharply and then decreases more slowly at higher concentrations. The minimum in the monomer emission does not coincide with the maximum in the excimer emission, and neither of them matches the value of the *cmc* of TX100 of about 0.26-0.27 mM [26,39].

As can be seen in the inset of Fig.3-a and in the normalized spectra (Fig.4) the spectral shift and the change in the shape of the spectra occurs in a narrow TX100 concentration interval around the cmc. Below about 0.2mM the intensity decreases, but the spectra do not change their shape (Fig.4, dashed orange curve)). This indicates that in this concentration interval the observed emission comes from the same species, namely free pyrene monomer, and that the observed quenching leads to a non-fluorescent species. Around the cmc, between 0.2 mM and 0.4 mM (Fig.4, dashed dotted green curve), follows a fast increase in intensity accompanied by a strong red shift in peak positions and a significant change in the shape of the spectrum. These spectral changes can only be explained by the contribution of at least two fluorescent species that are assigned to free and bound monomer. Above 0.4 mM the shape and position of the spectra stay again mostly constant.

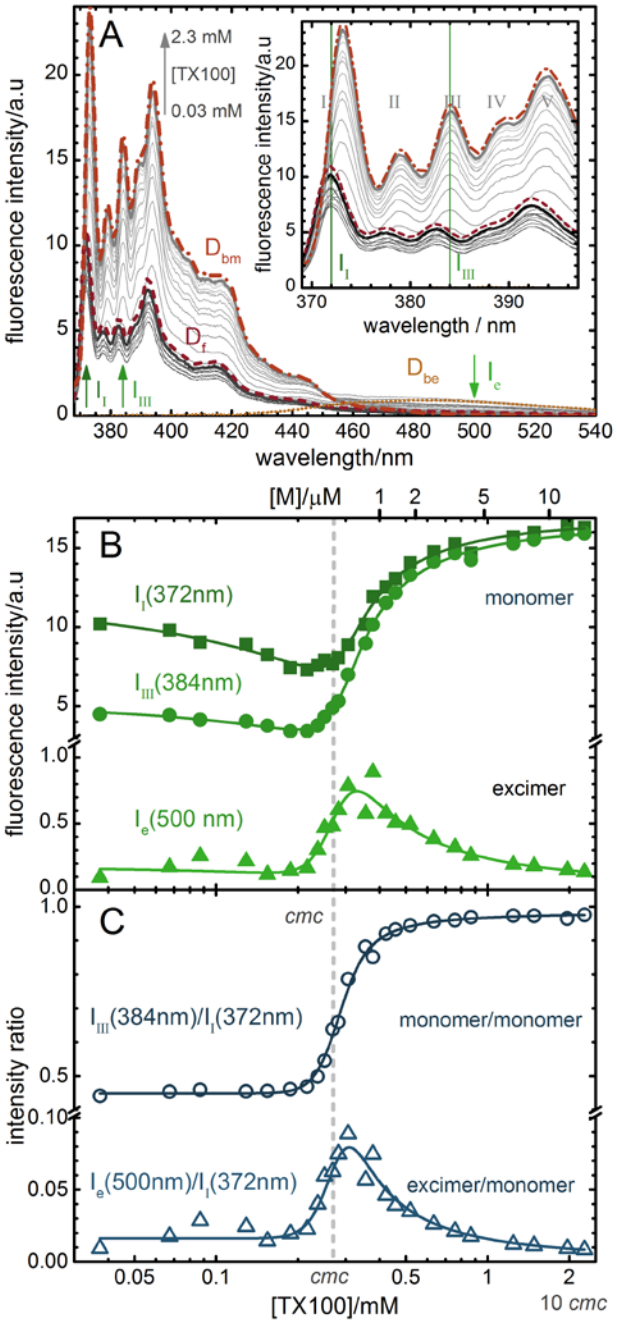

Fig.3: Fluorescence emission of pyrene in aqueous solutions of TX100, [TX100] = 0.03 mM – 2.3 mM. Panel A: Fluorescence spectra (thin grey curves) and pure spectra determined from PCGA (thick red dashed curves) of free pyrene (dashed), bound monomeric pyrene (dash dotted) and bound pyrene excimer (dotted). Inset: same as main panel with reduced wavelength scale. Panel B: fluorescence intensity in the monomer band, at peak I (371.9 nm, squares) and peak III (384.2 nm, circles) and in the excimer band at 500.0 nm, (triangles) as function of the TX100 concentration. Panel C: spectral ratios $SR_m^{(III,I)} = I_{III}/I_I$ (open circles) and $SR_e^{(e,I)} = I_e/I_I$ (open triangles). Thick curves in panels B and C: Global fit of equations (18), and (21), with the parameters given in the text. The dashed grey vertical line indicates the cmc. ([Pyrene]=5.2 10^{-7} M, λ_{exc}=319 nm). Note the logarithmic concentration scale and the breaks in the intensity scales.

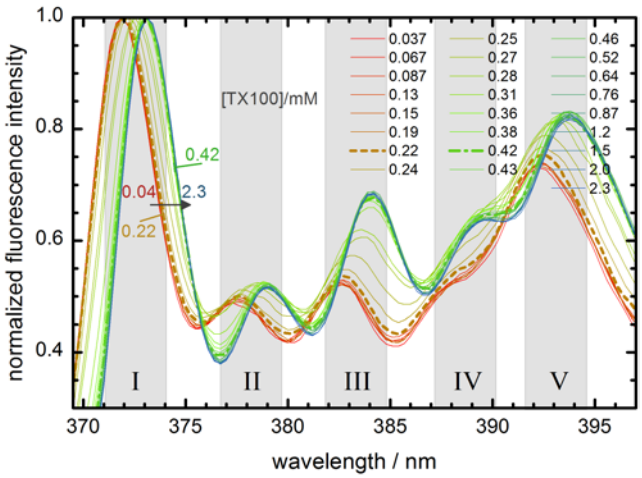

Fig.4: Normalized spectra of pyrene in TX100 solutions as shown in Fig. 3. The TX100 concentration increases from 0.04 mM (red) to 2.3 mM (blue), with 0.22 mM (dash, orange) and 0.42 mM (dashed dotted, green). Roman numbers and grey rectangles refer to the vibronic peaks in the pyrene spectrum.

Principal Component Analysis (PCA) [68,69] of the series of spectra confirms the presence of three fluorescent species in the concentration range studied here (see Figs. SI5 – SI7 in the SI). We assign them to free monomeric pyrene, D_f, bound monomeric pyrene, D_{bm}, and bound pyrene emitting as excimer, D_{be}. The observed spectra (or fluorescence intensities at given wavelength) are the sum of the contributions of these three species as given by eq (18). At low [TX100] only free dye D_f is present. The addition of TX100 quenches the fluorescence of free pyrene possibly due to formation of non-fluorescent surfactant-pyrene complexes (see section 3.3). Therefore the fraction of not quenched dye, X_{nq}, decreases with increasing [S_1] (eq. (17)) until the *cmc* is reached (see Fig.6-b). Above the *cmc* the value of X_{nq} stays constant since the concentration of monomeric surfactant does not vary ([S_1] = *cmc*).

At the onset of the formation of micelles, just before the *cmc*, a further small decrease in monomer emission is observed, which is not explained by the quenching process. In parallel a sharp increase in the excimer emission, I_e, is found. Both changes are due to the formation of pyrene excimer in higher occupied micelles near the *cmc* that do not emit in the monomer region.

As more and more pyrene molecules bind to micelles the emission in the monomer band is dominated by the higher emissive bound pyrene monomers, whereas the emission in the excimer band vanishes slowly as bound pyrene is distributed among the increasing concentration of micelles. Both the binding equilibrium and the distribution take place within a rather wide concentration interval from just below the *cmc* up to a multiple of it (note the logarithmic concentration scale in Fig. 3).

Table 1.

Results of global fits to the experimental data as indicated in the text.

	TX100	SDS
cmc / 10^{-3}mol ℓ$^{-1}$	0.275±.005	8.1±0.1
r	0.16±0.01	0.07±0.03
K / 10^3 mol ℓ$^{-1}$	3300±200	190±40
K_q / 10^3 mol ℓ$^{-1}$	2.2±0.2	0.23±0.03
$K_{be}^{'} = K_{be}V_m^{-1}$ / 10^3 mol^{-1}	0.6±0.3	3±1
n	143	64
τ_f / 10^{-9}s	124	127
k_m /10^6s^{-1} (τ_m / 10^{-9}s)	4.3 (232)	6.3 (160)
k_e /10^6s^{-1} (τ_e / 10^{-9}s)	9.8 (102)	34 (30)
$k_1^{'} = k_1V_m^{-1}$ / 10^6 mol^{-1}s^{-1}	2.4	20
τ_s / 10^{-9}s	5	4
$SR_f^{(2,1)}$ / $SR_{bm}^{(2,1)}$ / $q_{bm,f}^{(1)}$ / $q_{be,f}^{(e)}$ [a]	0.45/0.98/1.5/28	0.44/0.91/1.4/46
$SR_f^{(e,1)}$ / $SR_{bm}^{(e,1)}$ / $q_{be,f}^{(e,1)}$ [a]	0.016/0.004/0.37	0.020/.004/0.85
[M](*cmc*) [b]/ 10^{-6}mol ℓ$^{-1}$	0.12	3.5

[a] λ_1=372nm (peak I), λ_2=384nm (peak III), λ_e=500nm (excimer)

[b] Micelle concentration at the *cmc* estimated from eq.(7).

The surfactant concentration dependence of the pyrene fluorescence emission both in the monomer and in the excimer bands are very well described by the model of eq. (18) together with the concentration model of eq. (3). Global fits at three selected wavelength, 371.9 nm, 384.2 nm and 500.0 nm, are shown in Fig.3-b. Global fits of the whole series of spectra by PCGA are given in the SI. The best fit parameter values are given in Table 1. The corresponding fluorescence intensity ratios at 371.9 nm, 384.2 nm and 500.0 nm are $q_{bm,f}^{(\lambda)}$ =1.49, 3.26 and 0.42, and $q_{be,f}^{(\lambda)}$ =0, 0, 27, respectively. In the monomer bands the fit reproduces excellently the quenching at low TX100 concentration, the small "dip" just below the *cmc* due to the formation of excimer and then the sharp increase of the intensity after the *cmc*. Also the excimer band is very well described, both the sharp increase around the *cmc* and the approximately exponential decrease at higher concentrations. The fit determines a value of the *cmc* that is in very good agreement with that determined from the direct TX100 absorption (*cmc* = 0.270 mM) [39] and with other literature values [26]. The width of the transition region (*r*) is higher than the value *r*=0.11 obtained from the TX100 absorption but comparable to that determined for the exchange of other dyes with TX100- micelles [39]. The value of the binding equilibrium constant $K = 3.3\times10^6$ M^{-1} is very high and confirms the value published before [39].

Fig.3-c shows the spectral ratio $SR_m^{(\mathrm{III,I})} = I_{\mathrm{III}}/I_{\mathrm{I}}$ of the monomer intensities in peak I at 371.9 nm and peak III at 384.2 nm and the excimer-monomer ratio $SR_e^{(\mathrm{e,I})} = I_{\mathrm{e}}/I_{\mathrm{I}}$ between the excimer emission at 500 nm and the monomer peak I. The monomer ratio $SR_m^{(\mathrm{III,I})}$ is flat below the transition region up to about 0.2 mM, increases sharply between 0.2 and 0.4 mM and stabilizes at higher concentrations. The excimer ratio $SR_e^{(\mathrm{e,I})}$ shows a sharp increase just below the *cmc* followed by a peak and a less pronounced decay at higher concentrations. The concentration dependencies of these ratios are similar to those of the corresponding absolute intensities, but with some important differences (see Fig. 3-b and c). In the monomer ratio the effect of the pyrene-surfactant quenching is eliminated as discussed above (eq.(23)). Also the effect of the quenching due to excimer formation is mostly compensated so that the ratio increases much faster above the *cmc* than the corresponding intensities. Similarly, the peak in the excimer ratio is more symmetric than that of the intensity. The simpler form of the spectral ratios comes at a price, the loss of information. The spectral ratios are well fitted with eq. (21) using the parameters determined from the absolute intensities (Table 1). However, the fit of eq. (21) to the monomer ratio alone does not allow one to determine all parameters (*cmc*, *r*, *K*, $q_{bm,f}^{(1)}$, and K_q) independently due to the strong parameter correlation. This is not the case for fits of the absolute intensities, especially for simultaneous (global) fits at several wavelengths (peaks). Practical aspects of the determination of the *cmc* from pyrene spectral ratios will be subject of a following contribution.

The pyrene emission in solutions with increasing SDS concentrations behaves similarly to that of pyrene in TX100 solutions (Fig. 5). The main difference is the apparently more pronounced change near the *cmc* of the monomer intensities and of the monomer spectral ratio and the sharper peak of the excimer signals. Global fits of the model of eq. (18) together with the concentration model of eq. (3) at three selected wavelengths, 372 nm, 383 nm and 500 nm, are shown in Fig.5–a. The best fit parameter values are given in Table 1. The corresponding fluorescence intensity ratios at 372 nm, 383 nm and 500 nm are $q_{bm,f}^{(\lambda)}$ =1.36, 2.09 and 0.28 and $q_{be,f}^{(\lambda)}$ =0, 0, 46, respectively. The spectral ratios in the monomer and in the excimer bands are also well reproduced by eq. (21) using the parameters determined from the absolute intensities (Table 1). The concentration dependencies of selected parameters is are shown in Fig. 6 both for TX100 and for SDS.Again, the *cmc* does not coincide with characteristic points of the experimental data. It lies now clearly to the right of the mid-point of the monomer ratio and nearly in the middle of the excimer peak. The fit gives a *cmc* value which coincides with that determined from electrical conductivity [38]. The value of *r* agrees with that determined before (*r* = 0.11) but has a high uncertainy due to the low data quality just before the cmc.

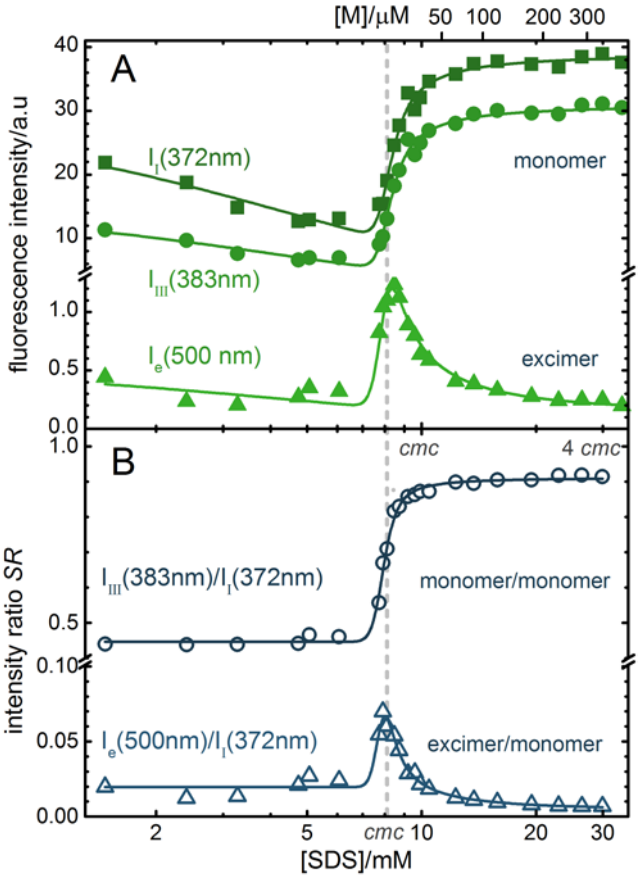

Fig. 5: Fluorescence emission of pyrene in aqueous solutions of SDS, [SDS] = 1.5 mM – 33 mM. Panel A: fluorescence intensity in the monomer band at peak I (372 nm, squares) and peak III (383 nm, circles) and in the excimer band at 500 nm, (triangles) as function of the SDS concentration. Panel B: fluorescence intensity ratios (spectral ratios) $SR_m^{(\mathrm{III,I})}$ =I372nm/ I(383nm)) (open circles) and $SR_e^{(\mathrm{e,I})}$ = I(500nm)/I372nm) (open triangles). Thick curves in panels B and C: Global fit of equations (18), (21) with the parameters given in the text. The dashed grey vertical line indicates the cmc. ([Pyrene]=1.5 10^{-6} M, λ_{exc}=319 nm). Note the logarithmic concentration scale and the breaks in the intensity scales.

We compare the fluorescence properties of pyrene in TX100 and SDS in Fig. 6 that covers the same concentration interval of $[S]_0$ = 0 – 2.5 *cmc* for both surfactants. The first row of panels (a, g) show the surfactant concentrations $[S_1]$, $[S_m]$, and [M] versus the total surfactant concentration $[S]_0$ (lower scale) and [M] (upper scale). Note the much higher micellar concentrations in the case of SDS. The second row (panels b, h) shows the fractions of free (X_f) and bound (X_b) pyrene, the fraction of not quenched free dye (X_f X_{nq}), and the fraction of monomeric dye (X_f + X_b X_{bm}). The mean occupancy $\bar{i}$ and the probability double or higher occupancy ($P_{i>1}$) are plotted in panels c and d. In the fourth row (panels d, j) the excimer fraction (X_{be}), the fraction of bound excimer (X_b X_{be}), and the fraction of bound monomer (X_b X_{bm}) are compared. Note the relatively high fraction of bound excimer up to several multiples of the *cmc*. Finally, the lower two rows show the influence of quenching and excimer formation on the fluorescence

intensity (I) and the spectral monomer ratio (SR_m) (see below).

Special attention deserves the value of the equilibrium constant K_{SDS} = 190 10^3 M^{-1} of pyrene in SDS micelles, which is 17 times smaller than the corresponding value in TX100 (K_{TX100} = 3300 10^3 M^{-1}). First, it is important to note that the affinity (solubility, partition) of pyrene to micelles depends strongly on the surfactant. The frequently found assumption of an "infinite" affinity to micelles has to be checked in each case. Second, the smaller K_{SDS} would be apparently in contradiction with the faster changes observed in the SDS data as compared to TX100 that seem to hint to a higher binding constant (compare Figs. 3-b and 5-a). This is of course a question of scales. The equilibrium constant K is defined as a function of the micelle concentration [M] (eq. (8)), but the experimental data are represented versus the total surfactant concentration $[S]_0$. Due to the much higher *cmc* (and the lower n) the SDS micelle concentration [M] increases much faster with $[S]_0$ than that of TX100. For example, at $[S]_0 = 2$ *cmc*, we have [M]≈1.8 µM for TX100, but [M]≈127 µM for SDS, 70 times higher ([M](2cmc) ≈ ($[S]_0$-*cmc*)/n = *cmc*/n, see the micelle concentration scale at the upper part of Figs. 3-b and 5-a). The complex dependence of [M] on $[S]_0$ near and above the *cmc* makes it difficult to interpret the fluorescence data in a representation versus $[S]_0$. And finally, for this data the *cmc* is smaller than the value determined from the fit of a Boltzmann function to the ratio $SR_m^{(III,I)} = I_1/I_{III}$, defined as $x_0+2\Delta x$ = 8.39 mM applying the criterion given by Aquiar et al. (see Fig. SI3 in the SI) [30]. The fits with the model equations presented here recover consistent values of the *cmc* without the need for additional assumptions or classifications.

It is important to be aware of the strong dependence of the absolute intensities and the spectral ratios on the processes of quenching and excimer formation. The lowest two rows of panels in Fig. 6 show simulated curves of the fluorescence intensity $I^{(\lambda)}([S]_0)$ (eq. (18)) and the spectral ratio $SR_m^{(2,1)}$ (eq. (21)) with the data of Table 1, but suppressing the effect of quenching (K_q = 0, orange dotted line), or of excimer formation (K_{be}=0, orange dashed dotted line), or both (green dashed line) (see also Fig. SI4 in the SI). Due to the formation of excimer (with $X_b \cdot X_{be}$, panels D and J) the monomer emission is partially quenched in the transition region (see the fraction of monomeric dye (X_f + X_b X_{bm}) in panels b and h) and, therefore, the onset of the monomer intensity curve is strongly displaced towards higher concentrations as compared to the case without excimer formation. Also the spectral ratio is affected with opposite effects of quenching and excimer formation. The dependence of I and SR_m on the excimer formation makes them also sensitively dependent on the total pyrene concentration. It is obvious that any method used to extract the *cmc* from these curves needs to take into account these different effects. It is not surprising that graphical analysis methods lead to differing *cmc* values depending on the experimental conditions and on the nature of the surfactant.

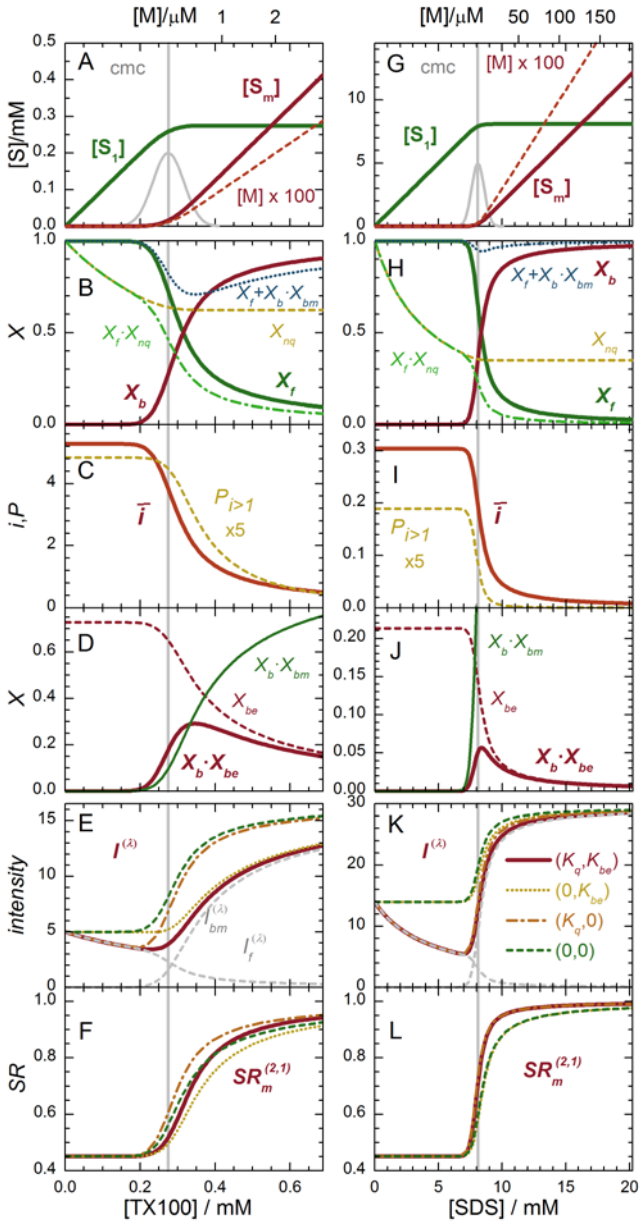

Fig.6: Surfactant concentrations [S_1], [S_m], [M] molar fractions X_f, X_{nq}, X_b, X_{be}, mean occupancy $\bar{i}$, occupancy probability $P(i>1)$, fluorescence intensity, and spectral ratio versus surfactant concentration [S_0] with the values of K and r determined for TX100 (panels A-F) and SDS (panels G-L) (see Table 1).

3.2 Time-Resolved Fluorescence Intensity

The time dependence of the fluorescence of pyrene in TX100 and SDS solutions after pulsed excitation is a complex function of the emission wavelength and surfactant concentration (Figs. 7 and 8). The fluorescence intensities in the monomer (390nm) and excimer (500nm) bands are very well fitted with eq. (26) and the parameters given in Table 1. In these global fits the values of *cmc*, r, K, and K_q were fixed to those obtained from the steady state data. The value of K'_{be} determined from the time-resolved data (see figure captions) coincide very well with those from the steady-state intensity (Table 1). The fluorescence in the monomer band of pyrene in TX100 solution shows a first fast decay with a lifetime of τ_s = 5 ns that is independent of [TX100] and is therefore attributed to the

fluorescence of the phenyl ring of TX100. A similar but much smaller contribution was observed in the case of SDS which is probably due to some fluorescent impurity. At concentrations below the *cmc* the monomer intensity decays monoexponentially with lifetime τ_f, independent on $[S]_0$. Similarly, at concentrations much above the *cmc* a single lifetime τ_m is found. In the transition region around the *cmc* the decays are more complex due to excimer formation but are very well described by eq. (26) (see Fig. SI1 in the SI), both in the monomer and in the excimer bands. The monomer intensity has a first faster decay corresponding to the formation of excimer in micelles of different occupancies and then a slower decay with τ_m. The excimer intensity grows first following the initial decay in the monomer intensity and then decays with τ_e. The excellent fits of time resolved and steady state data with the same set of parameter values corroborate the validity of the proposed models. Reported SDS excimer formation rates k_1 of $20 \cdot 10^6$ $M^{-1}s^{-1}$ are in good agreement with our value [8,55,70,71]. The lifetime of pyrene is quenched by oxygen both in water and within the micelles [72]. Our lifetime of free monomers and those bound to SDS micelles are slightly lower than those found for aerated solutions [72].

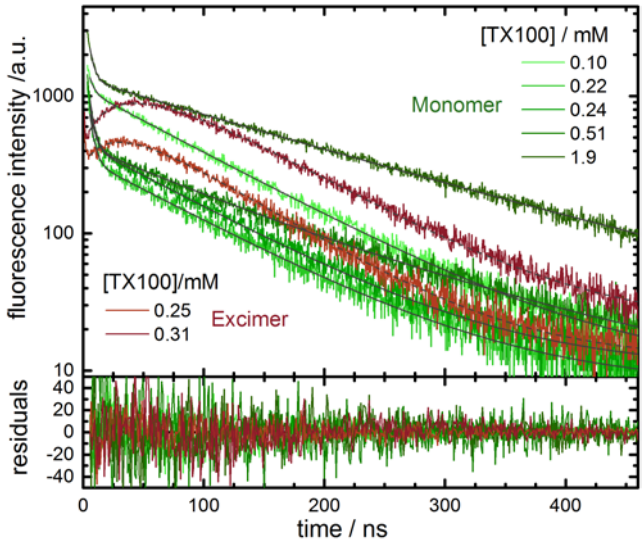

Fig.7: Time resolved fluorescence intensity of pyrene in aqueous TX100 solutions. Green thin curves: monomer band at 390 nm. Red thick curves: excimer band at 500 nm. Global fit with eq. (26) and parameters as given in the text $(K_{be}^{'} = (0.5 \pm 0.1)10^3\,\mathrm{mol}^{-1})$. Excitation at 300 nm. [Pyrene]=1.6 10^{-6} M for the monomer band and [Pyrene]=3.2 10^{-6} M for the excimer band.

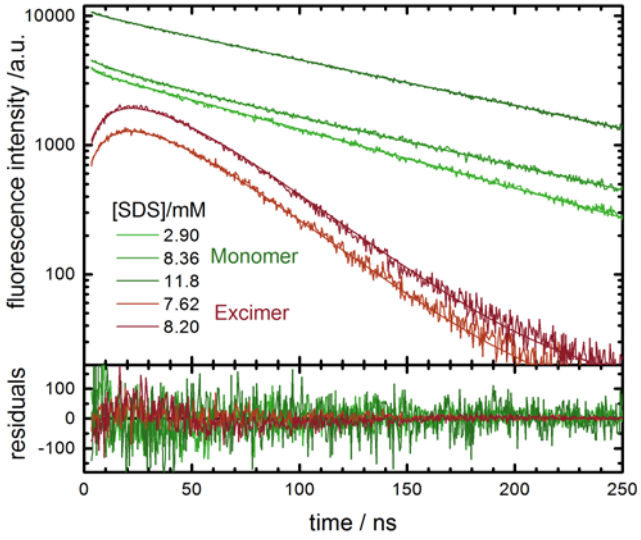

Fig.8: Time resolved fluorescence intensity of pyrene in aqueous SDS solutions. Green thin curves: monomer band at 390 nm. Red thick curves: excimer band at 500 nm. Global fit with eq. (26) and parameters as given in the text $(K_{be}^{'} = (4 \pm 1)10^3\,\mathrm{mol}^{-1})$. Excitation at 300 nm. [Pyrene]=3.2 10^{-6} M.

3.3 Pyrene-Surfactant Quenching

At low surfactant concentrations the fluorescence of pyrene decreases strongly upon addition of TX100 and to a lesser extent with SDS (Figs. 3 and 5), without shift in the position of the spectral peaks (Fig. 4). The observed decrease in fluorescence is well fitted as a (first order) quenching process between pyrene and free surfactant monomers as given in eqs.(16) and (17). Below the *cmc* the fluorescence of pyrene decays with a single lifetime which is independent of the surfactant concentration (τ_f in Table 1). This constant lifetime hints to static quenching in the ground state as the dominant process, as opposed to dynamic quenching, which would reduce the fluorescence lifetime. Static quenching is also in line with the increase of the solubility of pyrene in the presence of low surfactant concentrations as compared to pure water. Nevertheless, the stoichiometry and the nature of the pyrene-surfactant interactions are not clear. In the case of TX100 quenching probably occurs through formation of a ground-state non-fluorescent complex between the phenyl group of TX100 and pyrene, whereas SDS likely shows non-specific interactions with pyrene more appropriately described by the model of an effective sphere of quenching [45]. Nevertheless, at low quencher concentrations both types of static quenching and even the formation of complexes of higher quencher stoichiometries would lead to the same eq. (17) for the description of the steady-state fluorescence data. In conclusion, in order to infer the exact nature of the pyrene-surfactant interactions further studies should be performed which are beyond the scope of this work.

4 Conclusion

The complex photophysical behaviour of pyrene in surfactant solutions involves several processes that had been separately treated in detail in the past. The systematic

description of these processes in combination with a quantitative model for the surfactant concentrations allows us now to reproduce with high accuracy the behaviour of the steady-state and the time-resolved fluorescence intensity of pyrene in surfactant solutions near the *cmc*, both in the monomer and in the excimer emission bands. Our treatment yields concise model equations that can be used for the analysis of the pyrene fluorescence intensity in order to estimate fundamental parameters of the pyrene-surfactant system. We show how sensitively the pyrene fluorescence intensity depends on the binding equilibrium constant K of pyrene to a given surfactant micelle, on the rate constant of excimer formation in micelles k_1 (or K_{be}), and on the pyrene-surfactant quenching with K_q. The values K_{TX100} = 3300 10^3 M^{-1} and K_{SDS} = 190 10^3 M^{-1} for the binding of pyrene to TX100 and SDS micelles, respectively, are very high compared to other dyes [39], but not high enough to ignore the partition of pyrene even at relatively high surfactant concentrations above the *cmc*. The model offers also a solution to the notorious problem of the determination of the *cmc* from the pyrene fluorescence intensity, especially from the intensity ratio at two vibronic bands in the monomer emission or from the ratio of excimer to monomer emission intensity. Without further assumptions or ad hoc criteria we recover consistent values of the *cmc* of SDS and TX100 which are comparable with those determined from other techniques.

The precise determination of the *cmc* of a surfactant with the proposed model and pyrene as probe raises the question how the presence of a dye affects micelle formation and thus the exact position of the *cmc*. The quenching of the pyrene fluorescence and the much higher solubility of pyrene as compared to pure water show that pyrene and surfactant molecules interact already far below the *cmc*. Furthermore, near the *cmc* the concentration of bound pyrene is comparable to that of the micelles (mean occupancy $\bar{i} \approx 0.2 - 4$, see Fig. 6 and [M](*cmc*) in Table 1). We observe, however, that the values of the *cmc* of SDS and TX100 determined from the pyrene fluorescence coincide with those determined without dye, directly from the surfactant conductivity or absorbance [38,39]. The presence of hydrophobic pyrene molecules seems not to have a significant influence on the position of the *cmc* in these surfactants.

Finally we note that the finite width of the transition region below and above the *cmc* gives a plausible explanation for the appearance of significant concentrations of micelles already below the *cmc* and thus for the observed changes in the pyrene fluorescence in this region, without the need to postulate a species distinct from the proper micelles. We find thus no experimental evidence of premicellar aggregates or a shift of the *cmc* due to the presence of pyrene.

5 Experimental Section

5.1 Materials

Pyrene (Aldrich 42,642-3 (99%), CAS 129-00-0, Mw=202.26, used without further purification). The surfactants TX100 (Triton X-100, Fluka 93426, CAS 9002-93-1, Mw=646.85) and SDS (Sodium dodecyl sulphate, Sigma-Aldrich 436143, CAS 151-21-3, Mw 288.38 g/mol) were checked for potential fluorescence impurities and were used without further purification. Solutions were prepared using Milli-Q water.

Stock solutions of pyrene in ethanol were prepared by weighing. Aliquots of this pyrene stock solution were evaporated and the remaining dry thin film of solid pyrene was redissolved in a known volume of a concentrated surfactant solution ($[S]_0$>*cmc*) by prolonged stirring. Each sample was prepared freshly in 10 mL sample tubes by weighing each component and stirred about 30 seconds in a vortex just before measurement. In contrast to reports of other authors [73] we found significant changes in the spectral ratios and in the amount of excimer formed in the presence of trace amounts of ethanol in the samples.

5.2 Absorbance and Fluorescence Measurements

Steady-state fluorescence measurements were obtained with an Edinburgh-Instruments F900 spectrofluorimeter, equipped with a Xenon lamp of 450 W as excitation sources. The excitation wavelength was 319nm, lower than the typically used 337nm in order to avoid the overlap of the raman band with the first vibronic peak of pyrene. Slit widths of excitation and emission were 3nm and 0.5nm, respectively, with a digital resolution of 0.3 nm. Inner filter effects due to absorption by the surfactant at the excitation wavelengths can be excluded. For time-resolved fluorescence measurements the same F900 TCSPC-Spectrofluorimeter was used with pulsed LEDs (EPLED-300 and EPLED-345) for excitation. Decays in the monomer (excimer) band at 390nm (500nm) were excited at 300nm (345nm) with an emission slit of 10nm. All experiments were carried out at 25 ± 1 ºC.

5.3 Data Analysis

All data were analyzed with OriginPro 9.1 (*OriginLab Corporation*, US). All given uncertainties correspond to one standard deviation from the fits and do not include calibration errors. The Origin fit functions we used are given ready to use in the supplementary data. Time-resolved fluorescence intensities were either analyzed individually with the proprietary Edinburgh-Instruments Analysis software with excitation pulse deconvolution or globally in OriginPro 9.5 applying the model equations as tail-fits without deconvolution. Principal components global analysis (PCGA) of series of emission spectra was applied using a Mathematica (Wolfram Research, Champaign, IL) program developed by our group [68,69]. The model equations have been derived in Mathematica (Wolfram Research, Champaign, IL).

Acknowledgements

We thank Dr. Belén Reija for technical assistance. L.P. thanks the Xunta de Galicia for his research scholarships. M.N. and W.A. thank the Ministerio de Ciencia e Innovación and the Xunta de Galicia for their financial support (INCITE09262304PR, CTQ2010-21369, CN2012/314, GPC2013/052).

References

[1] Förster T, Selinger B. Der Konzentrationsumschlag der Fluoreszenz aromatischer Kohlenwasserstoffe in mizell-kolloidaler Lösung. Zeitschrift Naturforschung Teil A 1964;19:38.
[2] Graetzel M, Thomas J. The application of fluorescence techniques to the study of micellar systems. Modern fluorescence spectroscopy 1976;2:169-216.
[3] Kalyanasundaram K, Thomas JK. Environmental Effects on Vibronic Band Intensities in Pyrene Monomer Fluorescence and Their Application in Studies of Micellar Systems. J.Am.Chem.Soc. 1977;99:2039-44.
[4] Almgren M, Grieser F, Thomas Jk. Dynamic And Static Aspects Of Solubilization Of Neutral Arenes In Ionic Micellar Solutions. J.Am.Chem.Soc. 1979;101:279-91.
[5] Infelta PP, Graetzel M. Statistics of solubilizate distribution and its application to pyrene fluorescence in micellar systems. A concise kinetic model. J.Chem.Phys. 1979;70:179-86.
[6] Singer LA. Fluorescence Probes of Micellar Systems—An Overview. Solution Behavior of surfactants: Springer; 1982, p. 73-112.
[7] De Schryver F, Croonen Y, Geladé E, Van der Auweraer M, Dederen J, Roelants E, et al. Fluorescence Quenching in Micellar Systems. Surfactants in Solution: Springer; 1984, p. 663-672.
[8] Malliaris A. Fluorescence probing in aqueous micellar systems: an overview. International Reviews in Physical Chemistry 1988;7:95-121.
[9] Rharbi Y, Winnik MA. Solute Exchange Between Surfactant Micelles by Micelle Fragmentation and Fusion. Adv.Colloid Interface Sci. 2001;89:25-46.
[10] Capek I. Fate of excited probes in micellar systems. Adv.Colloid Interface Sci. 2002;97:91-149.
[11] Mohr A, Talbiersky P, Korth H, Sustmann R, Boese R, Bläser D, et al. A new pyrene-based fluorescent probe for the determination of critical micelle concentrations. The journal of physical chemistry.B 2007;111:12985-92, 10.1021/jp0731497.
[12] Mitsionis AI, Vaimakis TC. Estimation of AOT and SDS CMC in a methanol using conductometry, viscometry and pyrene fluorescence spectroscopy methods. Chemical Physics Letters 2012.
[13] Topel O, Cakir BA, Budama L, Hoda N. Determination of critical micelle concentration of polybutadiende-block-poly(ethyleneoxide) diblock copolymer by fluorescence spectroscopy and dynamic light scattering. Journal of Molecular Liquids 2013;177:40-3.
[14] Winnik FM. Photophysics of preassociated pyrenes in aqueous polymer solutions and in other organized media. Chem.Rev. 1993;93:587-614,10.1021/cr00018a001.
[15] da Graça Miguel M. Association of surfactants and polymers studied by luminescence techniques. Adv.Colloid Interface Sci. 2001;89–90:1-23.
[16] Varga I, Mészáros R, Makuska R, Claesson PM, Gilányi T. Effect of graft density on the nonionic bottle brush polymer/surfactant interaction. Langmuir : the ACS journal of surfaces and colloids 2009;25:11383-9,10.1021/la901499x.
[17] Lehrer SS. Intramolecular pyrene excimer fluorescence: a probe of proximity and protein conformational change. Methods Enzymol. 1997;278:286-95.
[18] Somerharju P. Pyrene-labeled lipids as tools in membrane biophysics and cell biology. Chem.Phys.Lipids 2002;116:57-74.
[19] Bains G, Patel AB, Narayanaswami V. Pyrene: a probe to study protein conformation and conformational changes. Molecules 2011;16:7909-35.
[20] Brea RJ, Vazquez ME, Mosquera M, Castedo L, Granja JR. Controlling Multiple Fluorescent Signal Output in Cyclic Peptide-Based Supramolecular Systems. J.Am.Chem.Soc. 2007;129:1653-7.
[21] Galla H, Sackmann E. Lateral diffusion in the hydrophobic region of membranes: use of pyrene excimers as optical probes. Biochimica et Biophysica Acta (BBA)-Biomembranes 1974;339:103-15.
[22] Vanderkooi JM, Callis JB. Pyrene. Probe of lateral diffusion in the hydrophobic region of membranes. Biochemistry 1974;13:4000-6.
[23] Wong M, Kulpa CF, Kerry Thomas J. Kinetic processes in< i> Escherichia coli</i> membranes and cells: A laser photolysis study using derivatives of pyrene. Biochimica et Biophysica Acta (BBA)-Biomembranes 1976;426:711-22.
[24] Dorrance R, Hunter T. Absorption and emission studies of solubilization in micelles. Part 1.—Pyrene in long-chain cationic micelles. J.Chem.Soc., Faraday Trans.1 1972;68:1312-21.
[25] Ananthapadmanabhan KP, Goddard ED, Turro NJ, Kuo PL. Fluorescence Probes for Critical Micelle Concentration. Langmuir 1985;1:352-5.
[26] Kalyanasundaram K. Photochemistry in Microheterogeneous Systems. New York: Academic Press; 1987.
[27] Anthony O, Zana R. Fluorescence Investigation of the Binding of Pyrene to Hydrophobic Microdomains in Aqueous Solutions of Polysoaps. Macromolecules 1994;27:3885-91.
[28] Regev O, Zana R. Aggregation behavior of Tyloxapol, a nonionic surfactant oligomer, in aqueous solution. J.Colloid Interface Sci. 1999;210:8-17.
[29] Caetano W, Tabak M. Interaction of Chlorpromazine and Trifluoperazine with Anionic Sodium Dodecyl Sulfate (SDS) Micelles: Electronic Absorption and Fluorescence Studies. J.Colloid Interface Sci. 2000;225:69-81,10.1006/jcis.2000.6720.
[30] Aguiar J, Carpena P, Molina-Bolivar JA, Ruiz CC. On the Determination of the Critical Micelle Concentration by the Pyrene 1 : 3 Ratio Method. J.Colloid Interface Sci. 2003;258:116-22.
[31] Israelachvili JN. Intermolecular and surface forces. 3rd ed. New York: Academic Press; 2010.
[32] Zana R. Dynamics of Surfactant Self-assemblies: Micelles, Microemulsions, Vesicles, and Lyotropic Phases. Boca Raton: Taylor & Francis/CRC Press; 2005.
[33] Blankschtein D, Shiloach A, Zoeller N. Thermodynamic theories of micellar and vesicular systems. Current opinion in colloid & interface science 1997;2:294-300.
[34] Stephenson BC, Beers K, Blankschtein D. Complementary use of simulations and molecular-thermodynamic theory to model micellization. Langmuir 2006;22:1500-13.
[35] Hadgiivanova R, Diamant H. Premicellar aggregation of amphiphilic molecules. J Phys Chem B 2007;111:8854-9.
[36] Sammalkorpi M, Sanders S, Panagiotopoulos A, Karttunen M, Haataja M. Simulations of Micellization of Sodium Hexyl Sulfate. The Journal of Physical Chemistry B 2011.
[37] Gezae Daful A, Baulin V, Avalos J, Mackie A. Accurate Critical Micelle Concentrations from a Microscopic Surfactant Model. The Journal of Physical Chemistry B 2011;115:3434-43.
[38] Al-Soufi W, Piñeiro L, Novo M. A model for monomer and micellar concentrations in surfactant solutions: Application to conductivity, NMR, diffusion, and surface tension data. J.Colloid Interface Sci. 2012;370:102-10,10.1016/j.jcis.2011.12.037.
[39] Piñeiro L, Freire S, Bordello J, Novo M, Al-Soufi W. Dye exchange in micellar solutions. Quantitative analysis of bulk

and single molecule fluorescence titrations. Soft Matter 2013;9:10779-90.
[40] Hauser M, Klein U. Excimere in micellaren Lösungen. Zeitschrift für Physikalische Chemie Neue Folge 1972;78:32-9.
[41] Nakajima A. Variations in the Vibrational Structures of Fluorescence Spectra of Naphthalene and Pyrene in Water and in Aqueous Surfactant Solutions. Bull.Chem.Soc.Jpn. 1977;50:2473-4.
[42] Glushko V, Thaler MS, Karp CD. Pyrene fluorescence fine structure as a polarity probe of hydrophobic regions: behavior in model solvents. Arch.Biochem.Biophys. 1981;210:33-42.
[43] Dong DC, Winnik MA. The Py scale of solvent polarities. Solvent effects on the vibronic fine structure of pyrene fluorescence and empirical correlations with ET and Y values. Photochem.Photobiol. 1982;35:17-21.
[44] Karpovich DS, Blanchard GJ. Relating the polarity-dependent fluorescence response of pyrene to vibronic coupling. Achieving a fundamental understanding of the py polarity scale. J.Phys.Chem. 1995;99:3951-8,10.1021/j100012a014.
[45] Valeur B, Berberan Santos MN. Molecular fluorescence: principles and applications. 2nd ed. Weinheim: Wiley VCH; 2012.
[46] Hauser M, Klein U. Fluorescence and Excimer Kinetics in Micellar Detergent Solutions. Acta Physica Et Chemica 1973;19:363-73.
[47] Selinger BK, Watkins AR. Distributional effects on excimer formation in micellar surfactant solutions. Chemical Physics Letters 1978;56:99-104.
[48] Selinger BK, Watkins AR. Pyrene excimer kinetics in micelles of nonionic surfactants. Journal of Photochemistry 1982;20:319-25.
[49] Turro NJ, Kuo PL. Pyrene excimer formations in micelles of nonionic detergents and of water-soluble polymers. Langmuir 1986;2:438-42.
[50] Tachiya M. Application of a generating function to reaction kinetics in micelles. Kinetics of quenching of luminescent probes in micelles. Chemical Physics Letters 1975;33:289-92.
[51] Maestri M, Infelta PP, Grätzel M. Kinetics of fast light-induced redox processes in micellar systems: Intramicellar electron transfer. J.Chem.Phys. 1978;69:1522-,10.1063/1.436724.
[52] Gehlen MH, De Schryver FC. Time-resolved Fluorescence Quenching in Micellar Assemblies. Chem.Rev. 1993;93:199-221.
[53] Ranganathan R, Vautier-Giongo C, Bales BL. Toward a Hydrodynamic Description of Bimolecular Collisions in Micelles. An Experimental Test of the Effect of the Nature of the Quencher on the Fluorescence Quenching of Pyrene in Sds Micelles and in Bulk Liquids. J Phys Chem B 2003;107:10312-8.
[54] Förster T. Excimers. Angewandte Chemie International Edition in English 1969;8:333-43.
[55] Malliaris A, Le Moigne J, Sturm J, Zana R. Temperature dependence of the micelle aggregation number and rate of intramicellar excimer formation in aqueous surfactant solutions. J.Phys.Chem. 1985;89:2709-13.
[56] Sahoo L, Sarangi J, Misra PK. Organization of amphiphiles, Part 1: Evidence in favor of pre-micellar aggregates though fluorescence spectroscopy. Bull.Chem.Soc.Jpn. 2002;75:859-65.
[57] Phillips J. The energetics of micelle formation. Transactions of the Faraday Society 1955;51:561-9.
[58] Dunaway CS, Christian SD, Scamehorn JF. Overview and history of the study of solubilization. In: Christian SD, Scamehorn JF, editors. Solubilization in Surfactant Aggregates, Surfactant Science Series, Vol. 55New York: Marcel Dekker; 1995, p. 3-31.
[59] Zana R. Dynamics in Micellar Solutions of Surfactants. In: Zana R, editor. Dynamics of Surfactant Self-assemblies: Micelles, Microemulsions, Vesicles, and Lyotropic PhasesBoca Raton: Taylor & Francis/CRC Press; 2005.
[60] Freire S, Bordello J, Granadero D, Al Soufi W, Novo M. Role of Electrostatic and Hydrophobic Forces in the Interaction of Ionic Dyes with Charged Micelles. Photochem. Photobiol. Sci. 2010;9:687-96.
[61] McNaught AD, McNaught AD. IUPAC Compendium of chemical terminology. Oxford: Blackwell Science; 1997.
[62] Dorrance RC, Hunter TF. Absorption and emission studies of solubilization in micelles. Part 2.—Determination of aggregation numbers and solubilisate diffusion in cationic micelles. J.Chem.Soc., Faraday Trans.1 1974;70:1572-80.
[63] Hunter TF. The distribution of solubilisate molecules in micellar assemblies. Chemical Physics Letters 1980;75:152-5.
[64] Thomas JK. Radiation-induced reactions in organized assemblies. Chem.Rev. 1980;80:283-99.
[65] Moroi Y. Distribution of solubilizates among micelles and kinetics of micelle-catalyzed reactions. J.Phys.Chem. 1980;84:2186-90.
[66] Kim J, Domach MM, Tilton RD. Effect of Electrolytes on the Pyrene Solubilization Capacity of Dodecyl Sulfate Micelles. Langmuir 2000;16:10037-43,10.1021/la0005560.
[67] Tachiya M. Kinetics of quenching of luminescent probes in micellar systems. II. J.Chem.Phys. 1982;76:340.
[68] Al-Soufi W, Novo M, Mosquera M. Principal component global analysis of fluorescence and absorption spectra of 2-(2'-hydroxyphenyl)benzimidazole. Appl.Spectrosc. 2001;55:630-6.
[69] Al-Soufi W, Novo M, Mosquera M, Rodríguez-Prieto F. Principal Component Global Analysis of Series of Fluorescence Spectra. Reviews in Fluorescence 2009 2011:23-45.
[70] Lianos P, Viriot ML, Zana R. Study of the solubilization of aromatic hydrocarbons by aqueous micellar solutions. J.Phys.Chem. 1984;88:1098-101,10.1021/j150650a014.
[71] Villegas MM, Neal SL. Model-independent analysis of pyrene photokinetics in SDS micelles. The Journal of Physical Chemistry A 1997;101:6890-6.
[72] Geiger MW, Turro NJ. Pyrene fluorescence lifetime as a probe for oxygen penetration of micelles. Photochem.Photobiol. 1975;22:273-6.
[73] Kim J, Domach MM, Tilton RD. Pyrene solubilization capacity in octaethylene glycol monododecyl ether (C12E8) micelles. Colloids Surf.Physicochem.Eng.Aspects 1999;150:55-68.